COHERENCE AND WAVELENGTH EFFECTS ON THE GROWTH MECHANISM OF POROUS SILICON NANO-STRUCTURES

by

Aslı Çakır SAYGILI

B.S., Physics Engineering, Ankara University, 2000

Submitted to the Institute for Graduate Studies in
Science and Engineering in partial fullfilment of
the requirements for the degree of
Master of Science

Graduate Program in Physics
Boğaziçi University
2009

ACKNOWLEDGEMENTS

I would like to express my sincere gratitude to Professor Naci İnci for submission of the subject, for his suggestions in the development of this study and for his invaluable guidance and help during the preparation of this dissertation.

I would like to thank Assistant Professor Bükem Bilen for her guidance in the development of this study.

I would like to thank Professor Yani Skarlatos for his precious suggestions for the final editions of this thesis.

Thanks to research assistant Sabriye Açıkgöz for providing valuable technical assistance during the labotarory work.

Thanks to Dr. Bilge Gedik Uluocak and Dr. Sinan Şen for providing AFM and ESEM images and for suggestions for the final editions of this thesis.

And finally, thanks to my husband Assistant Professor Altuğ Saygılı for his support during the preparation and organization of the final draft of this thesis.

ABSTRACT

COHERENCE AND WAVELENGTH EFFECTS ON THE GROWTH MECHANISM OF POROUS SILICON NANO-STRUCTURES

In this study, the objective is first to produce regular porous silicon(PS) nano-structures and then to observe the effects of wavelength and coherence length of the light, which is used for illumination, on the growth mechanism of these structures. P^+ type silicon wafers are exposed to various light sources, both coherent and incoherent. Lasers with different wavelengths are used to compare the wavelength effects and light emitting diode is employed to compare the effects of coherence lenght on the porous silicon's growth mechanism. The nanocrystalline silicon samples formed in the electrochemical dissolution are characterized in terms of optics and structure. An optical characterization method is used to analyze the origin of nanocrystal silicon luminescence and radiative recombination mechanism. Optical characterization is also capable to show if the porous nano-structures are formed or not. Optical results are supported by structural characterization methods; such as AFM (Atomic Force Microscope) and ESEM (Environmental Scanning Electron Microscope). In these methods, images, taken from each sample at different magnifications, denote characteristics of formed pores such as size and shape.

ÖZET

UYUM UZUNLUĞU VE DALGA BOYUNUN GÖZENEKLİ SİLİKON NANO-YAPILARIN OLUŞUMU ÜZERİNDEKİ ETKİLERİ

Bu çalışmadaki amaç öncelikle düzenli gözenekli silikon nano-yapılar oluşturmak, daha sonra bu yapıların aydınlatılması için kullanılan ışığın dalgaboyunun ve uyum uzunluğunun silikon nano-yapılar üzerindeki etkilerini gözlemlemektir. P^+ tipinde silikon tabakalar hazırlanmış ve silikon tabakalar nano yapıların oluşumu esnasında farklı ışık kaynaklarına maruz bırakılmıştır. Dalgaboyunun gözenekli silikon oluşumu üzerindeki etkisini kıyaslamak amacı ile farklı dalgaboylarındaki lazerler, uyum uzunluğunun gözenekli silikon oluşumu üzerindeki etkisini kıyaslamak için de mavi led kullanılmıştır. Elektrokimyasal solüsyon içerisinde oluşturulan nanokristal yapıdaki silikon numuneler optik ve yapısal açıdan karakterize edilmiştir. Nanokristal silisyum ışımasının kaynağının ve ışınımsal yeniden birleşim mekanizmasının analiz edilmesi amacı ile optik karakterizasyon metodu kullanılmıştır. Optik karaterizasyon metodu aynı zamanda gözenekli nano-yapıların oluşup oluşmadığını gösterme kabiliyetine sahip bir tekniktir. Optik sonuçlar, AFM (Atomik Kuvvet Mikroskobu) ve ESEM (Çevresel Taramalı Elektron Mikroskobu) yapısal karakterizasyon metotları kullanılarak desteklenmiştir. Bu metotlarda, her örnekten farklı büyütmelerde alınan görüntüler, oluşan gözeneklerin boyut ve şekil gibi karakteristik özelliklerini göstermektedir.

TABLE OF CONTENTS

LIST OF FIGURES

LIST OF TABLES

LIST OF SYMBOLS/ABBREVIATIONS

μm	Micrometer
nm	Nanometer
J	Current Density
J_{ep}	Electropolishing Current Density
AFM	Atomic Force Microscopy
BPF	Band Pass Filter
BSE	Back Scattered Electron
ESEM	Environmental Scanning Electron Microscopy
HF	Hydrofluoric Acid
HPF	High Pass Filter
PS	Porous Silicon
PL	Photoluminescence
SE	Secondary Electron
LED	Light Emitting Diode

1. INTRODUCTION

There is a world wide interest in porous silicon due to its optical and structural properties. Since the highly porous nanostructure in the silicon gives rise to quantum confinement of charge carriers, porous silicon emits efficient visible light at room temperature, on the contrary crystalline silicon has indirect bandgap and does not have efficient light emission. With the discovery of the efficient luminescence from the nanostructured porous silicon by Canham, both laser diodes and transistors took a big step forward [1]. The PS is suitable for applications of the sensing devices such as optical and gas sensors and light-emitting devices like photodetectors and solar cells. Moreover, one of the recent applications, compatibility with human tissue had evoked a great interest. But to utilize from PS in technology, the size, shape and density of the nanostructures should be controlled independently.

Method of manufacturing PS nanostructures vary such as electrochemical anodization, stain etching and chemical vapor deposition, but controlling the size and shape of the nanostructures have remained troublesome. Many parameters affect formation of the nanostructures such as resistivity, silicon type, anodization time, current density and illumination.

Porous silicon was realized during electropolishing of silicon with hydrofluoric acid contained electrolyte. Until today, there have been many studies to create ordered, regular nano-pores and to understand the mechanism of the photoluminescence from PS [2,3,4]. Laser illuminated PS studies have been practised mostly by Kolasinski et al. [5] Spontaneous formation of conical structures at the surface of the PS were achieved with the femtosecond and nanosecond pulsed laser irradiation under appropriate conditions. Consequently, for short wavelength irradiation , pillars were formed at 10-25 μm with 3-4,5 μm tips. Pillars formed with long wavelenght laser does not have sharp tips as much as short wavelength [5]. The size of the pillars respond to the wavelenght of the laser and more densely packed pillars were formed at 390 nm compared with 780 nm by Kolasinski and Mills [6].

The aim of this study is to introduce and search the optical and structural properties of the porous silicon nanostructures which have been achieved by chemical anodization of p-type silicon wafers and assisted to lasers with different wavelenghts, white light and blue led. Consequently, to achieve regular nano-pillars on the surface of the laser illuminated silicon and to see the effects of the wavelength and coherence length on the PS nanostructure formation is intended.

The layout of the thesis is in the following sequence; a general information about the growth mechanism of the porous silicon, luminescence theory and coherence length is given in chapter 2. In chapter 3, experimental procedure of PS formation, optical and structural characterization methods and experimental setup components are mentioned. Also, the obtained results which are obtained from photoluminescence (PL) spectroscopy, environmental scanning electron microscopy (ESEM) and atomic force microscopy (AFM) are analyzed. Finally, in chapter 4, conclusion is given.

2. REVIEW

2.1. Growth Mechanism of Porous Silicon

There are two different ways of forming porous silicons (PS). The procedures are anodization and stain etching. In the anodization method, porous silicon is formed by the electrochemical dissolution of silicon wafers in an HF ethanoic solution [7]. This dissolution is achieved by controlling either the potential or anodic current. Constant current is most preffered for better control of the porosity and reproducibility of PS. The simplest anodisation cell is shown in Figure 2.1 in which silicon wafer is used as anode and any HF-resistant, such as platinum or stainless steel, is used as cathode. Also the cell is composed of an HF resistant material such as plexiglass or teflon. The advantage of this anodisation cell is its simplicity, but it has a disadvantage that is the inhomogeneity of formed pores, since the current flowing througth the silicon wafer is different at points A and B. The current density drops across the wafer, therefore the non-uniform pores and thickness differences are seen on the surface.

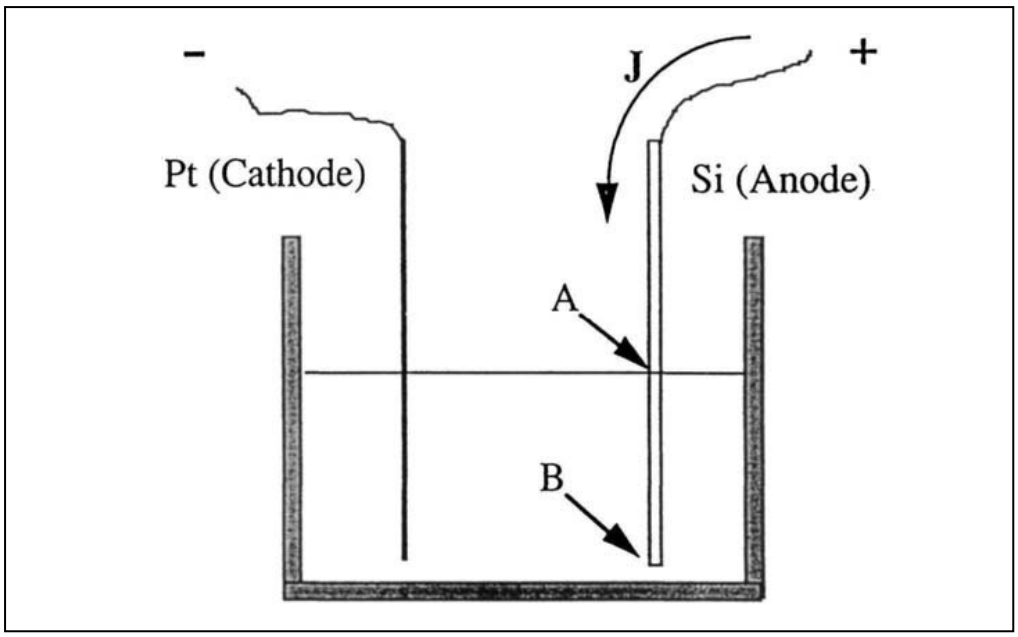

Figure 2.1. Cross-sectional view of the basic anodization cell

The second type of the anodisation cell is a single tank cell which is shown in Figure 2.2. In this type, only front side of the silicon wafer is exposed to the HF, back side is used as a metallic contact for conductivity. The single tank cell is prefered for illumination of the sample during anodisation and for producing uniform porous silicon samples. The high dose metalic back side contact is needed for silicon which has high resistivity typically higher than few mΩ, on the other hand, silicon with less than few mΩ resistivity can be used without the metalic contact [8].

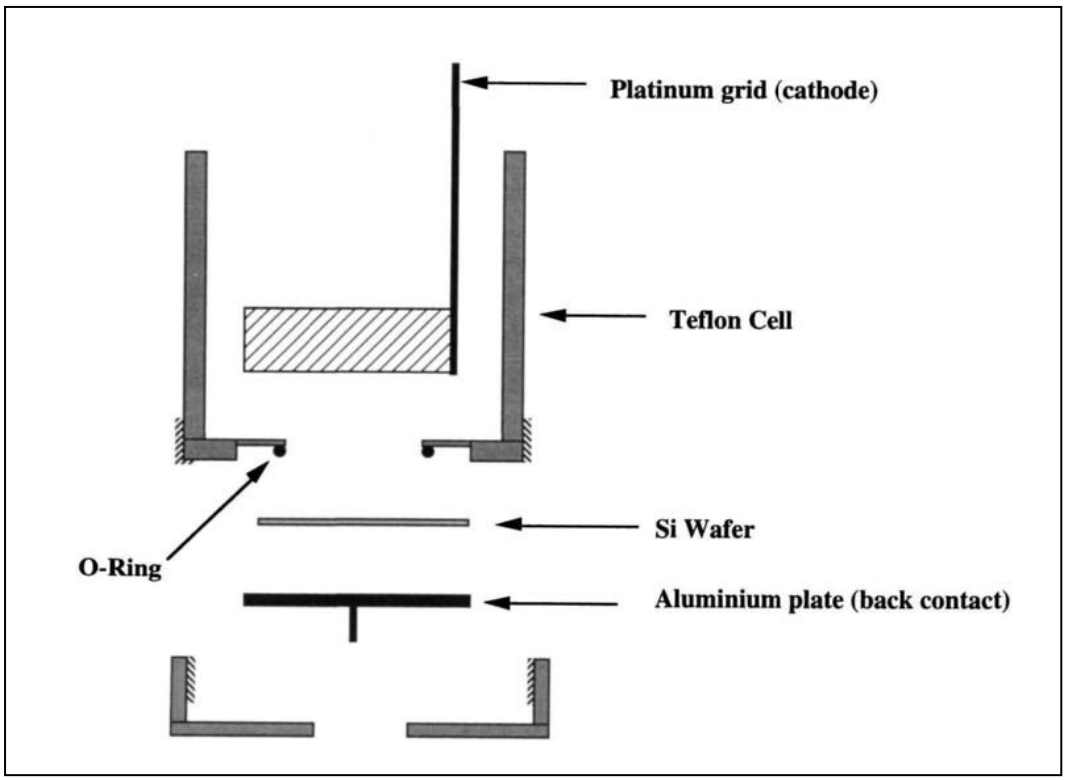

Figure 2.2. Single tank cell

The third type of the anodisation cell is the double tank cell. As shown in Figure 2.3, two stainless steel plates are used as anode and cathode and current flows from one cell through the silicon to another cell. Two side of silicon is exposed to the HF solution and pores are formed at the front side, since front side of the silicon acts as second anode. Thanks to the circulation of electrolyte via the pumps, the hydrogen bubbles, which occur as a result of proton reduction to the back side of the silicon, are removed from the cell [9].

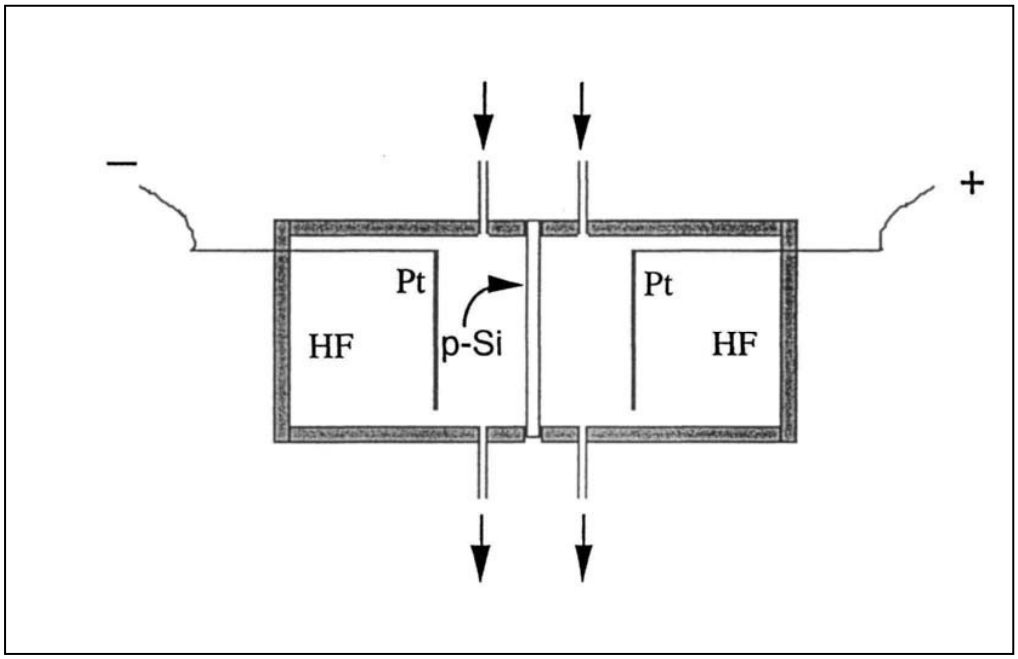

Figure 2.3. Cross sectional view of the double tank cell

Porous silicon can also be produced by stain etching which is simpler than the anodisation process but is a less frequently used method. There are some drawbacks of stain etching when compared to the anodisation process, which are lower photoluminescence efficiencies, worse homogeneity in pores and difficulties in reproducibility [10].

There are some key parameters which effect the formation of the porous silicon. The solution composition is one of the most important parameters. There is hydrogen evolution during porous formation. When pure HF solution is used in the formation, hydrogen bubbles stick to the surface of the silicon and induce inhomogeneity. To eleminate the hydrogen bubbles and achieve homogen porous structure, it is necessary to add absolute ethanol in HF. The ethanol consentration should not be less than 15%. Another important parameter is the current density flowing through the silicon. In Figure 2.4, a typical J-V curve for p^+-silicon is shown [8]. The current density-voltage curve is like Shottky diode as expected for semiconductor-electrolite interface [11]. Current density should be smaller than the electropolishing current density (J_{ep}) for the pore formation. J_{ep} separates the porous silicon formation region from the electropolishing region. Some other parameters which effect the PS formation are wafer type, resistivity, anodisation time and drying conditons.

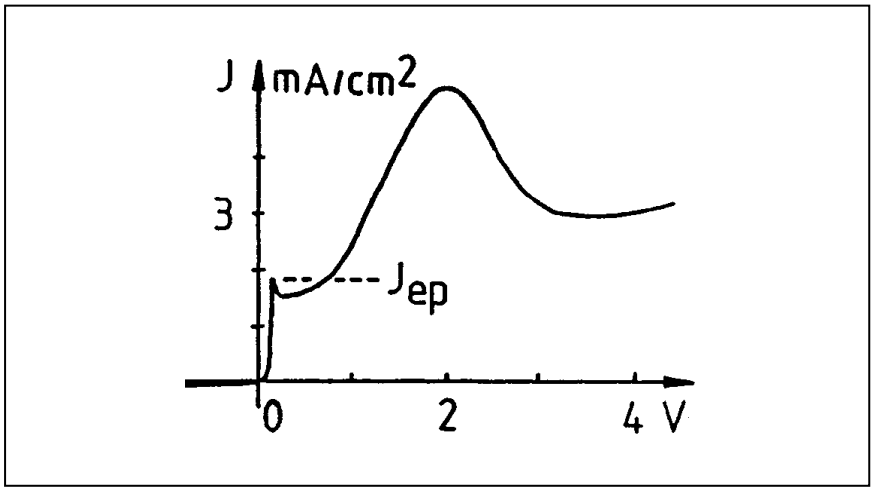

Figure 2.4. J-V curve for p^+-silicon

After etching, drying process plays an important role to achive a homogen PS. Cracks occur at the surface of the PS during the drying stage of the sample due to the stress associated with the evaporation from the pores. There are different drying techniques, such as pentane drying, supercritical drying, slow evaporation and freeze drying. Pentane drying, which is one of the easiest methods to perform, reduce capillary tension. Pentane does not interact with PS. Supercritical drying is the most efficient method to reduce cracks but is complicated and expensive to implement, therefore other drying techniques are more prefered. It was first carried out by Canham [8]. PS is dipped in a suitable liquid such as carbon dioxide and heated above the critical point, afterwards the gas is removed by liquid. In the freeze drying technique the PS is frozen at a temperature around -500 F and sublimed under vacuum. Slow evaporation method includes the water and ethanol rinsing.

2.2. Luminescence Theory

2.2.1. Recombination and Luminescence

Semiconductors have two types of bandgaps, which are direct and indirect. In direct bandgap, the lowest energy state of the conduction band and the highest energy state of the valance band have the same k–vektor, on the contrary, the indirect bandgap in which the

minimum energy of the conduction band and maximum energy of the valance band have different k-vectors [12].

Luminescence from a semiconductor occurs with electron-hole pair recombination with the result of a released photon which has an energy equal to the bandgap energy. In this case radiative recombination probability is large and the radiative lifetime is short (about a few nanoseconds). This process is possible in a direct bandgap material. For light emission in an indirect bandgap semiconductor such as silicon, electron-hole radiative recombination must involve a phonon absorption or emission as well as a photon release. There will be both energy and momentum change in this process, thus radiative lifetime is in the milisecond range with very low radiative recombination rate. Illustration of the direct and indirect bandgap luminescence theory is shown in Figure 2.5. [13].

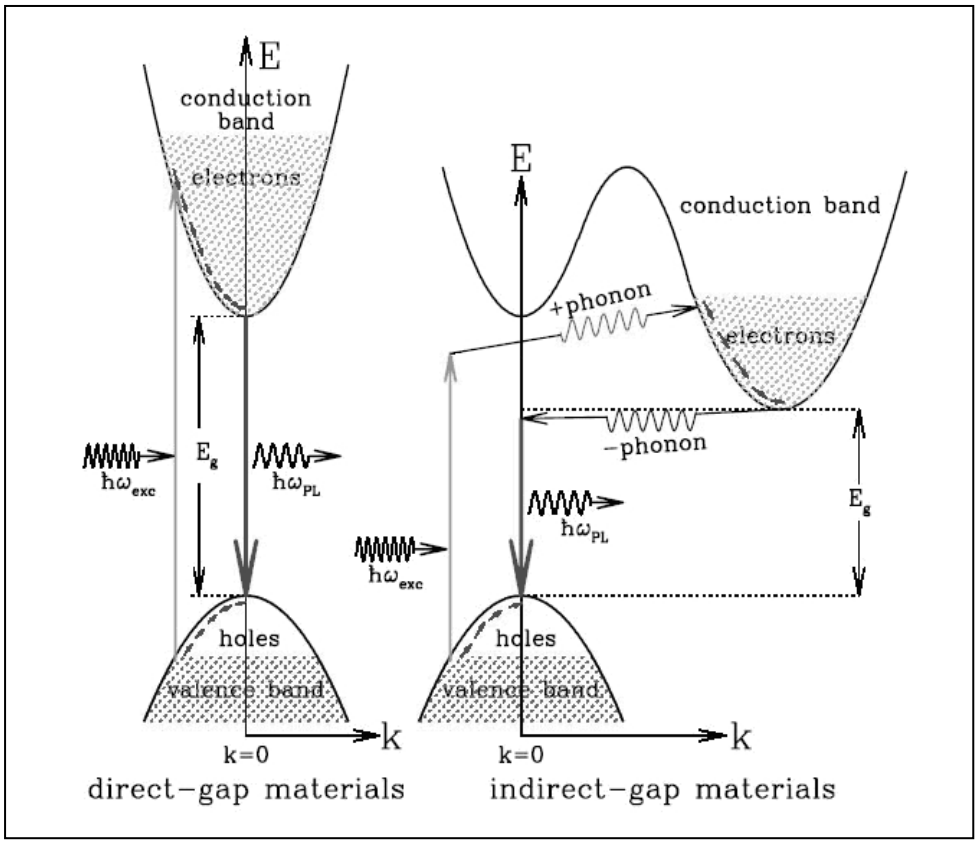

Figure 2.5. Luminescence from direct and indirect bandgap semiconductors

Non-radiative recombination is another process in which the electron's energy is transferred to the defects or impurities. The total radiative lifetime is given by:

$$\frac{1}{\tau} = \frac{1}{\tau_{rad}} + \frac{1}{\tau_{nonrad}} \tag{1}$$

The luminescence efficiency, defined as the ratio of the emitted photon number to the number of excited electron-hole pair [15], determined by the competition between radiative and non-radiative recombination. Luminescence efficiency is given by:

$$\gamma = \frac{\tau_{nonrad}}{\tau_{nonrad} + \tau_{rad}} \tag{2}$$

In an in-direct bandgap materials, radiative recombination rate is low, which means that the small portion of the total recombination is radiative recombination, therefore non-radiative part is more dominant. Thus, luminescence efficiency can be increased either by lower radiative lifetime or higher non-radiative lifetime [14].

2.2.2. Quantum Confinement Effect

For particles in the nanometer size, photoluminescence(PL) efficiency and PL peak energy change due to the quantum confinement effect. When the particle wavelength is small compared to the confining dimension, it behaves like a free particle. Thus, bandgap of the material remains at its original energy because of the continuous energy state. Conversely, when the confining dimension decreases at a certain limit such as nanometer scale, electrons and holes are confined and their motion is quantized in all dimensions. Consequently, energy spectrum turns to discrete and the bandgap energy E_g is increased, as shown in Figure 2.6. The confinement of the particles introduces an uncertainty in its momentum due to the Heisenberg's uncertainty relation $\Delta x \Delta p \geq \hbar/2$. Excitons are catched by impurities and PL spectrum shows discrete steps at low temperatures. In nanostructured silicon, confined carriers have higher energy than the free carriers therefore the nanocrystal silicon has a wider bandgap.

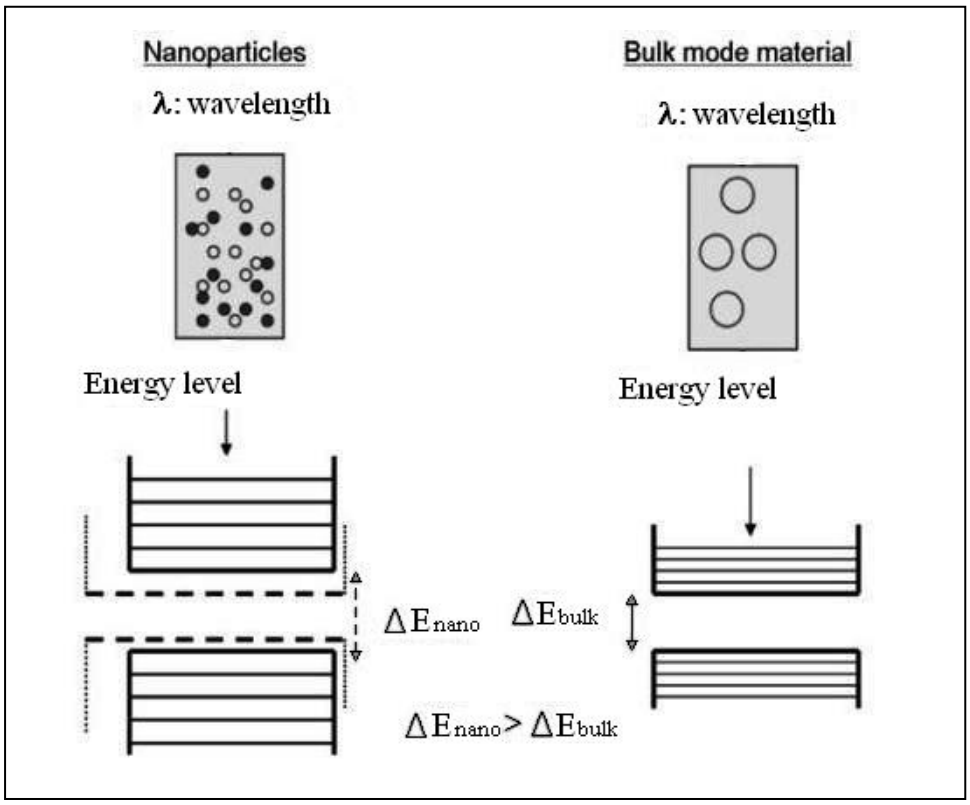

Figure 2.6. Increase in the bandgap energy due to quantum confinement

2.3. Coherence Length and Wavelength

A sinusodial wave periodically extends and can be considered as infinite at the same amplitude and same frequency. Such a sine wave is perfectly coherent since at all points of the wave coherence is predictable. But a pure sine wave is far from reality, in application a wave exists over a finite time duration Δt, is known as coherence time and this time corresponds to a finite wave train length which is $\ell = c\Delta t$. The coherence time Δt is a consequence of the electron transitions for generation of light is on the order of 10^{-8} or 10^{-9} second [16]. Since wave trains are finite, there will be a number of frequencies in its spectrum which is centered around ν_0 over a range $\Delta\nu$ band width or spectral width, as shown in Figure 2.7 [17]. The coherence time-spectral width correlation is given by

$$\Delta\nu = \frac{1}{\Delta t} \tag{3}$$

and the coherence length is given by

$$\ell = c\Delta t = \frac{\lambda^2}{\Delta\lambda} \tag{4}$$

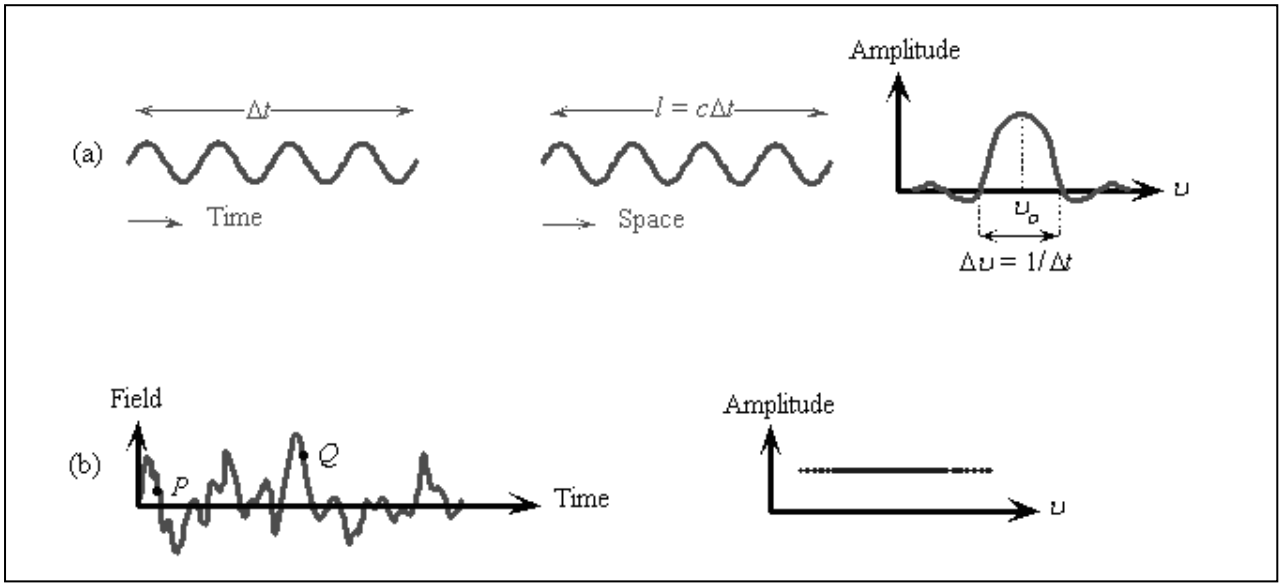

Figure 2.7. A finite wave train and its spectrum (a), white light wave (b)

Light waves from laser devices have important coherence lengths. A He-Ne laser operating in multimode has red lasing emission with a spectral width around $1.5\text{x}10^{9}$ Hz. This means that its coherence time is $\Delta t=0.67\text{x}10^{-9}$ second and corresponding coherence length is about 200mm. On the other hand, white light exhibits almost no coherence as seen in Figure 2.7.b.

3. EXPERIMENTAL STUDY

3.1. Sample Growth

PS samples are prepared by electrochemical anodization of p-type silicon wafers in HF:C_2H_5OH(1:1) solutions under white light, laser with different wavelengths and blue led. The clean silicon wafers are first cut into pieces and back surfaces of the silicon pieces are coated with aluminium as thin film contacts by evaporation in Edwards Coating System E306A. The silicon samples are dipped into HF:C_2H_5OH solution after the copper wires are attached to the aluminium films at the back of the silicon samples with silver paste. The copper wire is connected to the positive terminal of the power supply and the stainless steel is connected to the negative terminal as shown in Figure 3.1 [18]. The current is kept constant during anodization. Both the current density (J) and the time are important parameters to create the regular pillars and obtain the intense photoluminescence [19].

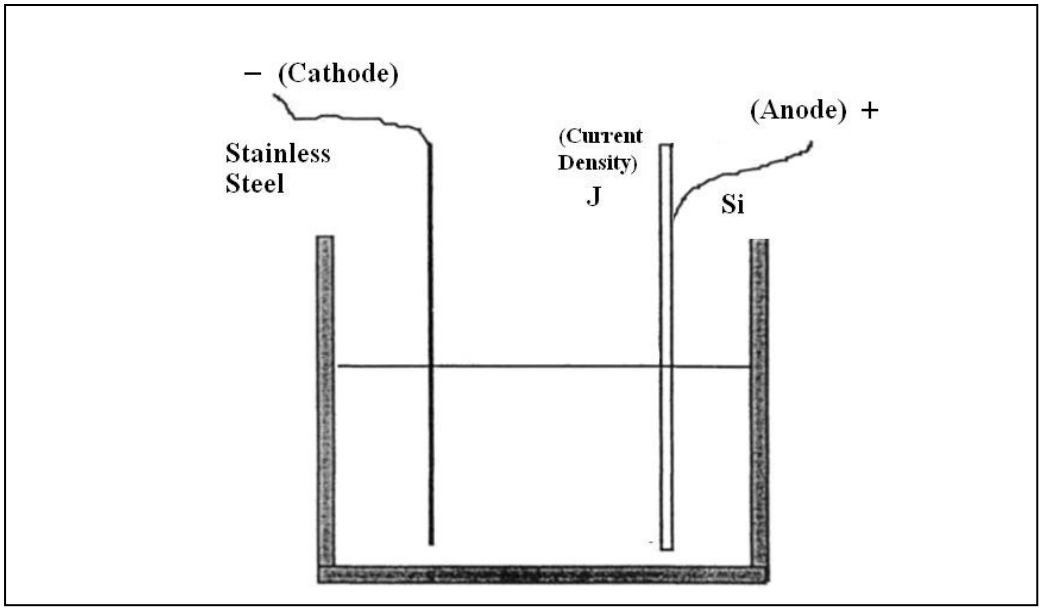

Figure 3.1. Electrochemical anodization of p-type silicon wafer

Samples are illuminated during anodization with different light sources: four lasers with different wavelengths, blue led and white light source. Two of the used lasers were Picoquant PDL 800-D Pulsed Diode lasers with wavelengths 467 nm(blue one) and 405

nm(purple one), one of the other used laser is Spectra-Physics Pulsed Hydrogen laser with 337 nm wavelength and Thorlab He-Ne laser is red pulsed with 633 nm. Blue led and white light source are used apart from the lasers. All laser sources are used to investigate the effects of the wavelength on the PS growth mechanism. Blue diode laser and blue led are used to see the coherence length effect onto the PS formation. In Table 3.1, wavelength values are seen for all laser sources which are used for illumination and in Table 3.2, wavelength and coherence length values of the blue laser and blue led are given.

Table 3.1. Wavelength values for all laser sources

	He-Ne laser(red)	Diode laser (blue)	Diode laser(purple)	Hydrogen laser
λ (nm)	633	467	405	337

Table 3.2. Wavelength and coherence length values of blue laser and blue led

	λ (nm)	Δλ (nm)	l (mm)
Diode laser (blue)	467	0,01	180
Blue led	440	100	0,002

3.2. Optical Characterization

Optical characterization is a nondestructive and contactless photo-excitation method which allows to probe the sample with various excitation wavelength for a range of the penetration dephts. In this work, photoluminescence is employed to characterize the samples.

3.2.1. Photoluminescence and Optical Setup

In a photoluminescence process, material absorbs photons and then re-radiates photons. This is the reverse process of the absorption. With the photon radiation, an excited

electron in an excited state returns to the initial state. The energy of the emitted photon is equal to the bandgap energy of the material. In an indirect bandgap material, phonon assisted photoluminescence occurs, thus bandgap energy is given by,

$$\hbar\omega = E_g \pm \hbar\Omega \tag{5}$$

Ω is the frequency of absorbed or emitted phonon and ω is the frequency of the incident photon. Throughout the excited light absorption, electrons in the conduction band and holes in the valance band is produced in semiconductors, than electrons and holes combine to restore the equilibrium. Electron-hole pair recombination occurs very quickly, typically life time of electron-hole pair is about 10 nanoseconds [20,21].

The photoluminescence spectroscopy which is shown in Figure 3.2 is used to obtain the emission spectra of the porous silicon. In this setup, an ultraviolet pulsed laser head with a wavelength of 405 nm is used as the excitation source. The laser head is driven by a picosecond diode driver (PDL 800-B Picoquant) at 40 MHz repetition rate. The separated fluorescence emission and the excitation occur at the dichroic mirror, which is placed at 45^0 to the laser head, reflects the excitation light towards a microscope objective(Nikon ELWD 50X). Throughout the microscope, the excitation light is focused onto the sample. After the excitation light is emitted from the fluorescent sample, it is filtered out from two spectral filters which are Band-Pass Filter (BPF) and High-Pass Filter (HPF) used to prevent any stray light from excitation beam. Finally, a fiber optic spectrometer (USB4000-VIS-NIR Ocean Optics) is used to monitor the fluorescence emission. The experiments are carried out at room temperature and in a dark environment.

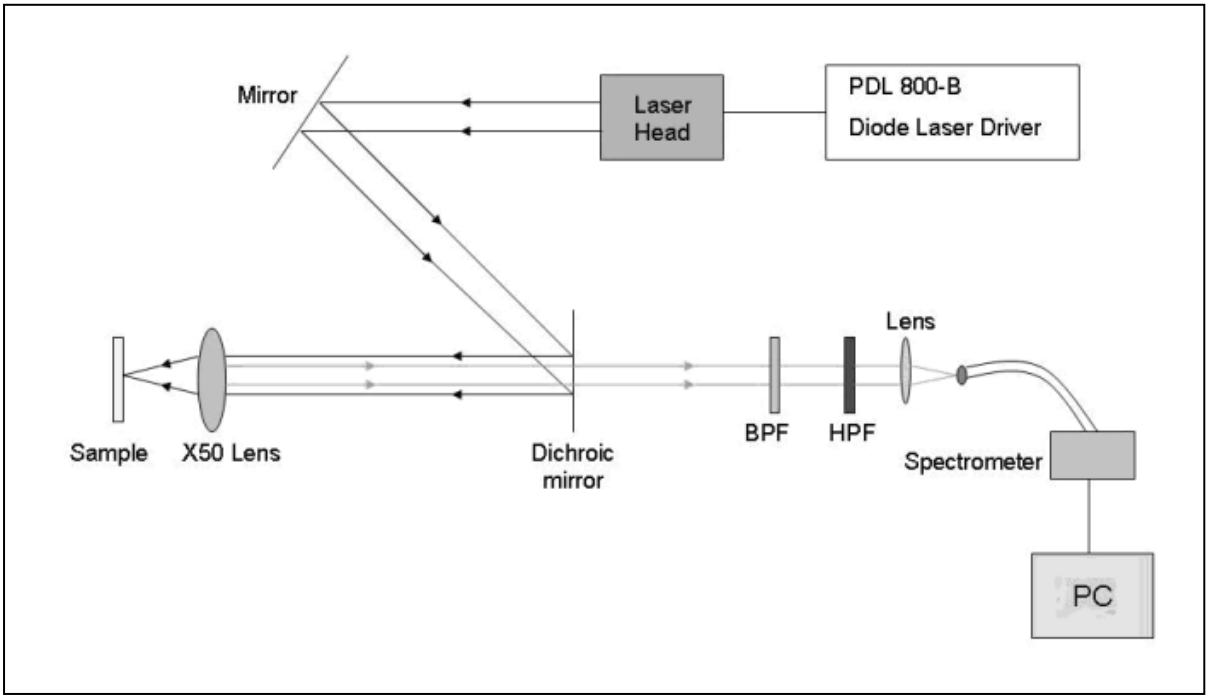

Figure 3.2. Optical setup of the luminescence spectroscopy.

3.3. Structural Characterization

Surface morphology of all porous silicon samples are investigated by Environmental Scanning Electron Microscopy (ESEM) and all PS samples which are exposed to the white light and blue led are characterized by Atomic Force Microscopy (AFM).

3.3.1. Environmental Scanning Electron Microscopy

Environmental Scanning Electron Microscopy (ESEM) provides high resolution image in nanoscale by electron beam technique. The electrons interact with the atoms corresponding to the specimen that make up the sample producing signals that include information about the sample's surface morphology. Difference of the Environmental SEM is the presence of water vapour for non-metalic and biological uncoated samples since this materials collect the charges and blaze. In a typical SEM , after an electron beam is emitted from an electron gun, it is focused by one or two condenser lenses. When focused beam interacts with the sample, the energy exchange between beam and sample gives rise to the electrons with high-energy. These electrons are detected as various types of signals and transferred to the topographical surface image, schematic drawing of ESEM is shown in

Figure 3.3. Two of them are secondary electrons (SE) and back scattered electrons (BSE). In secondary electron imaging, electron atom interaction occurs at the surface or near the surface and image gives information about the surface structure. In back scattered electron imaging, the beam electrons are reflected from sample and BSE image provides information about the composition of the sample surface. In this study, Philips ESEM-FEG/EDAX microscope is used to image the silicon pillars.

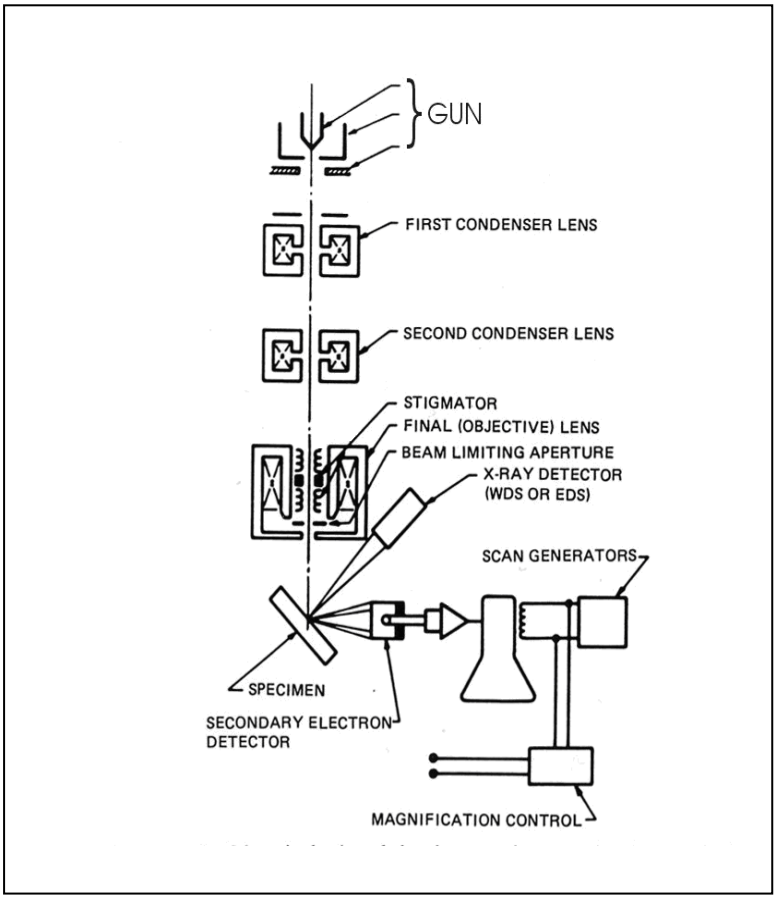

Figure 3.3. Schematic drawing of the ESEM.

3.3.2. Atomic Force Microscopy (AFM)

Atomic Force Microscopy gives the topographic map of the sample surface by scanning a sharp probe tip mounted on a cantilever. The vertical displacement of the tip lead to deflections of the cantilever, which are monitored by a laser beam focused at the end of the cantilever. The basic objective of the operation of AFM is to measure forces at atomic level between a sharp tip and sample surface. As the tip scans the surface of the

sample, by moving up and down with contour of the sample, laser beam is deflected from the attached cantilever into a dual element photodiode which measures the difference in light intensities and convert them to the voltage. The working principle of the AFM is shown in Figure 3.4. There are two different scanning modes which are tapping and contact modes. In the tapping mode, cantilever is oscillated at its resonant frequency(60-400 kHz) and scans across the sample surface. In the contact mode, the tip makes physical contact with the sample surface and scans across the sample while a feadback loop maintains a constant cantilever deflection and force. In this study, Ambios USPM model AFM is used and all images were taken at the tapping mode.

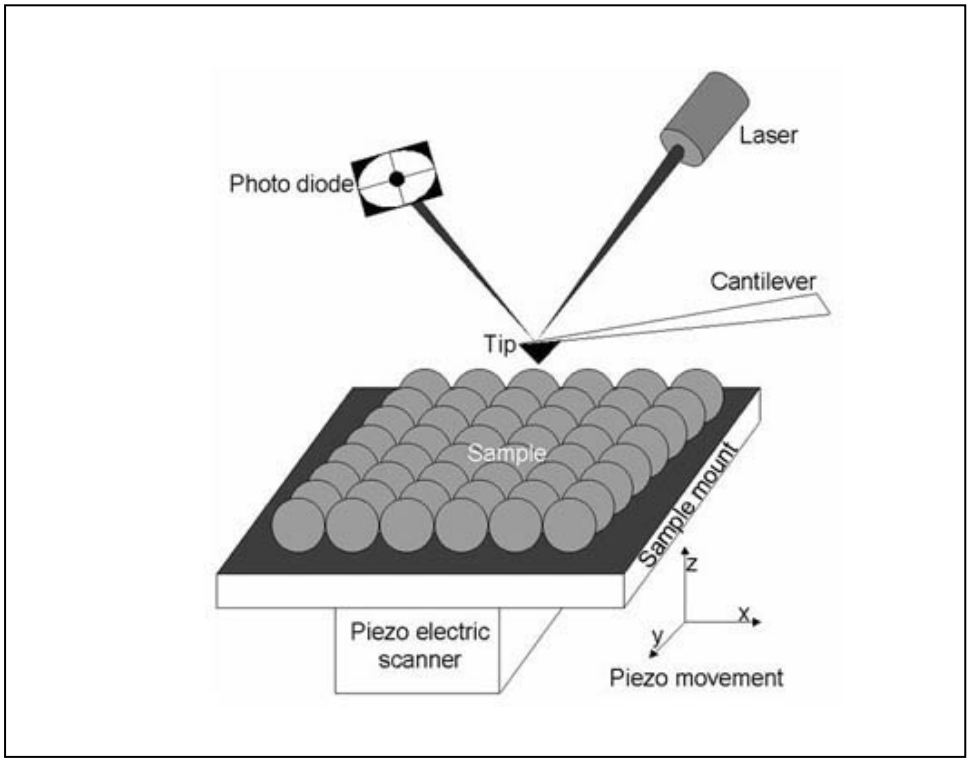

Figure 3.4. Working principle of atomic force microscopy.

3.4. Results and Discussion

PS samples are characterized by photoluminescence spectroscopy and surface images are taken by environmental scaning electron microscopy and atomic force microscopy.

Photoluminescence experiments mentioned in the section 3.2 are performed for all PS samples in a dark environment and at room temperature. Photoluminescence spectra are

shown in Figures 3.5, 3.6, 3.7, 3.8, 3.9 and 3.10 taken from PS samples which are illuminated with hydrogen, blue, purple, red lasers, blue led and white light respectively. According to these PL spectra, samples have porous structures in the nanometer scale, hence they give luminescence peaks around the same wavelength due to the quantum confinement effect. There are intensity differences in the PL peaks. Peak intensities of the blue led and white light illuminated samples are higher than that of the hydrogen, He-Ne and diode lasers. The reason of the intensity differences in PL can be understood from ESEM images. The white light and blue led illuminated PS samples have a denser nanostructure. On the contrary, laser assisted PS samples are formed as pillars and luminescence occurs at the tips of the pillars. When the tips of the pillars are taken into account, laser assisted PS samples do not have a dense nanostructure like that of white light and blue led assisted PS samples.

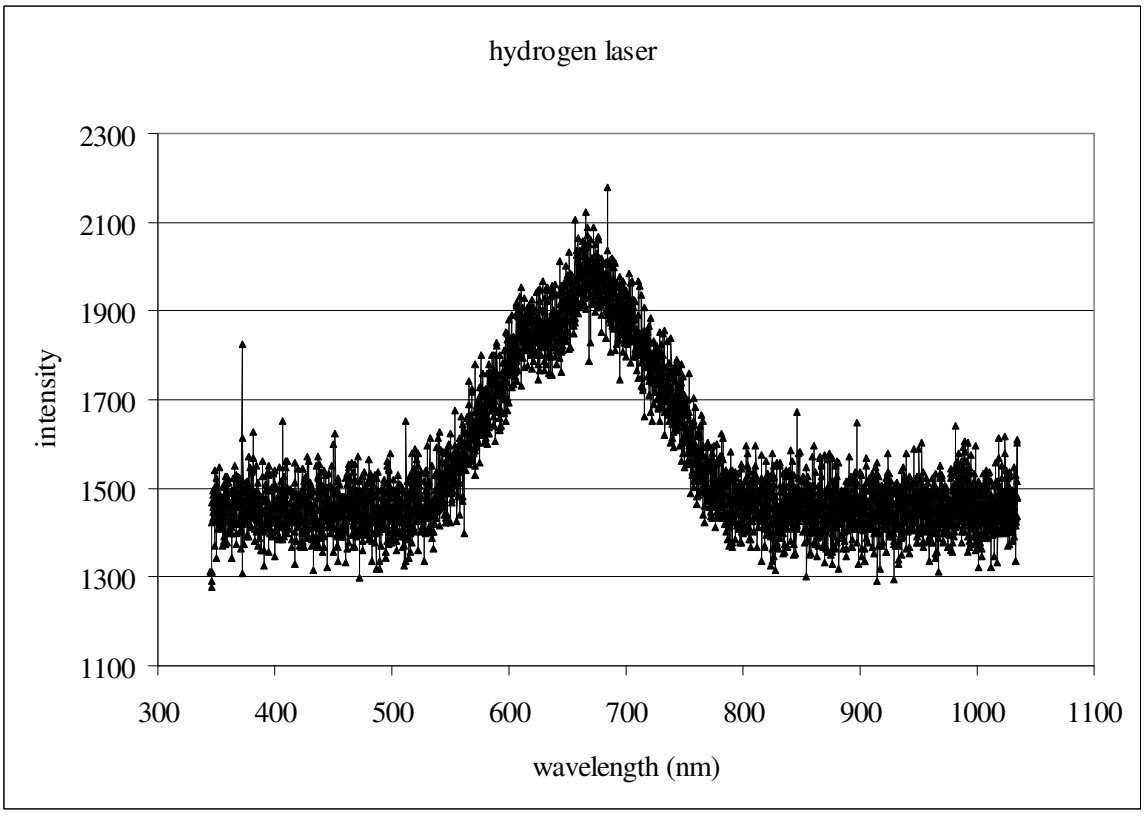

Figure 3.5. PL spectrum of the PS samples exposed to the hydrogen laser source.

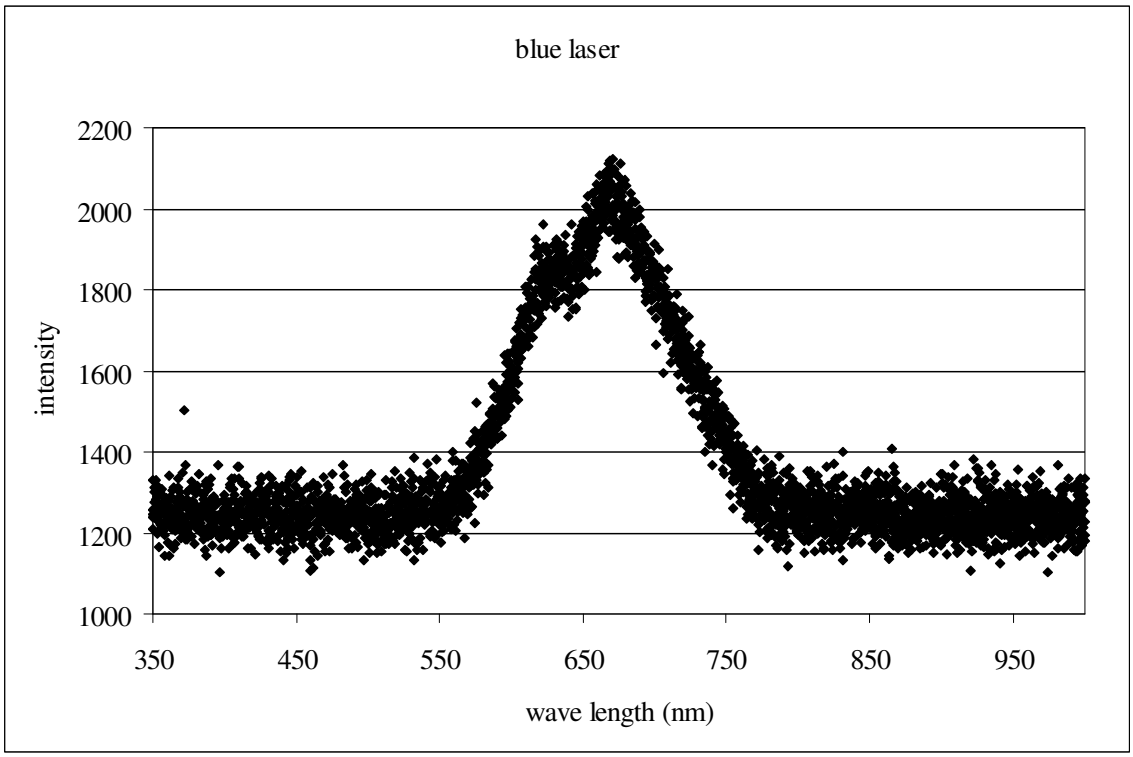

Figure 3.6. PL spectrum of the PS samples exposed to the blue laser source.

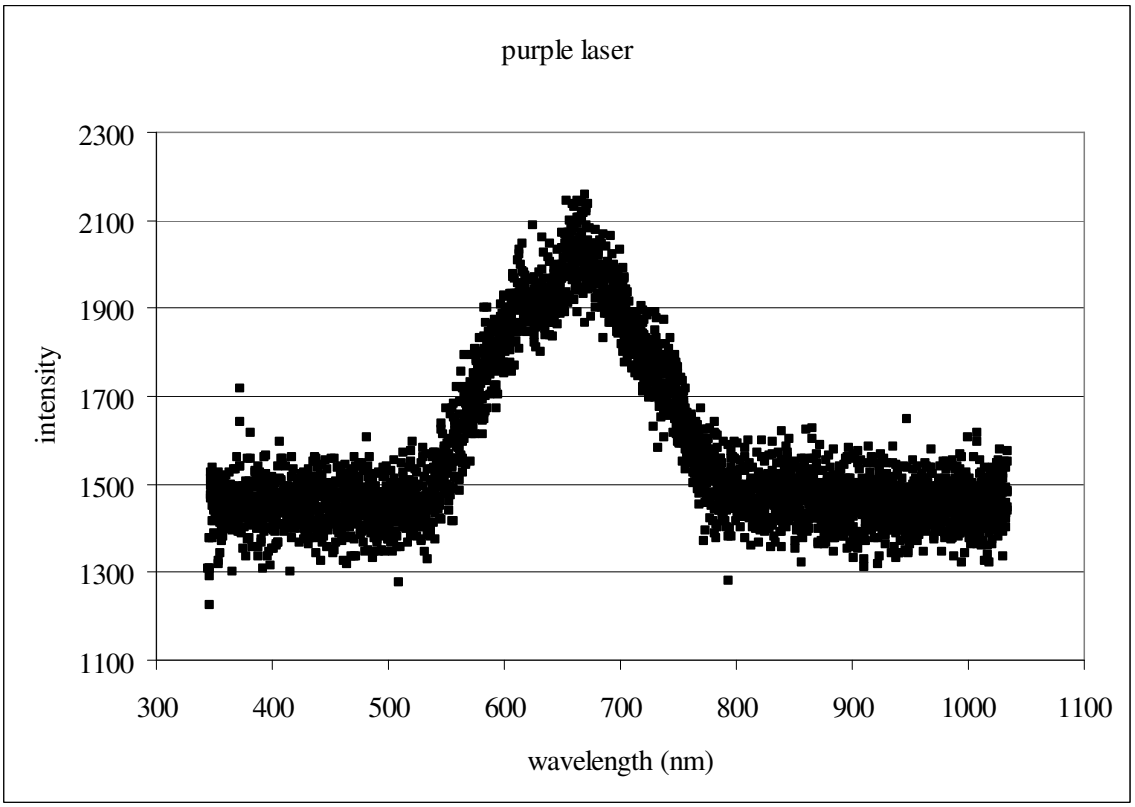

Figure 3.7. PL spectrum of the PS samples exposed to the purple laser source.

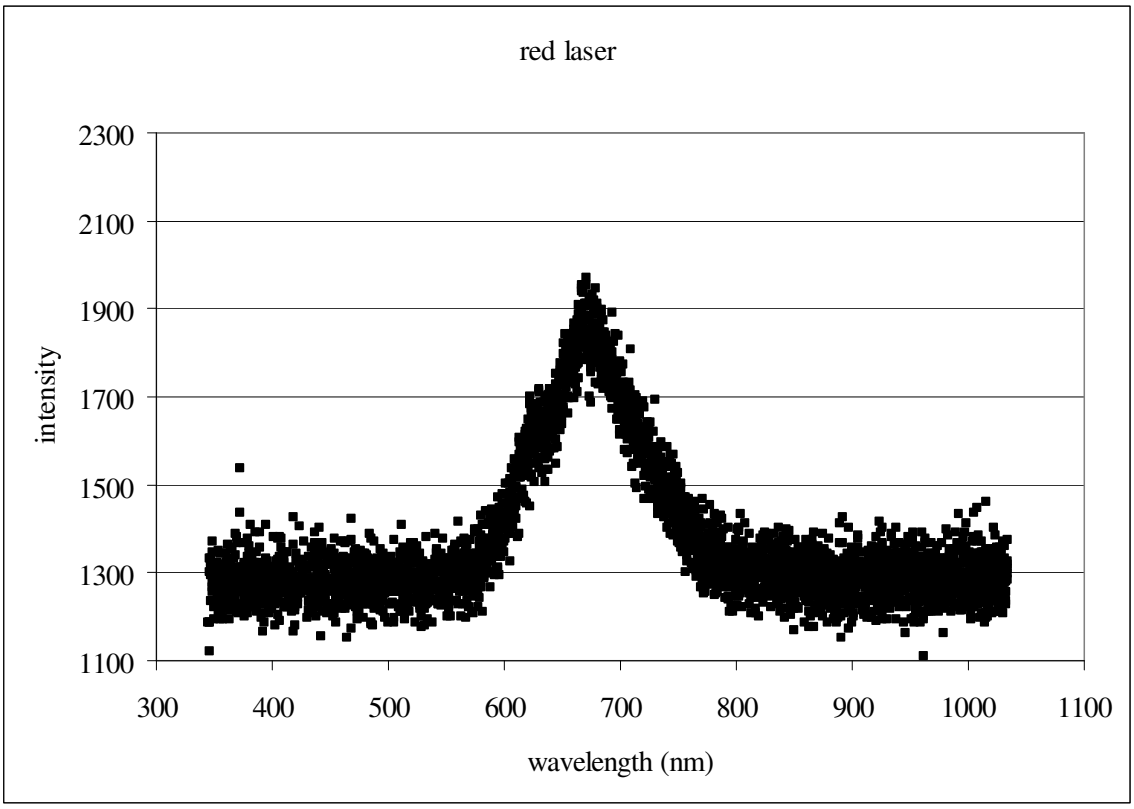

Figure 3.8. PL spectrum of the PS samples exposed to the red laser source.

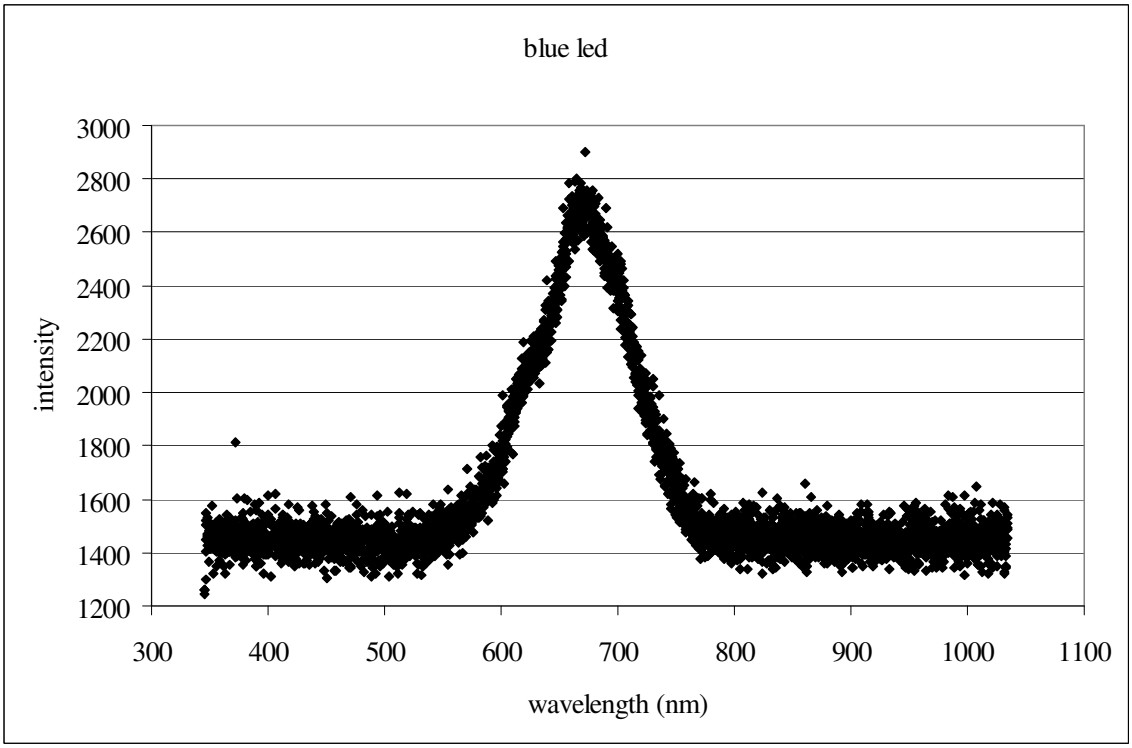

Figure 3.9. PL spectrum of the PS samples exposed to the blue led source.

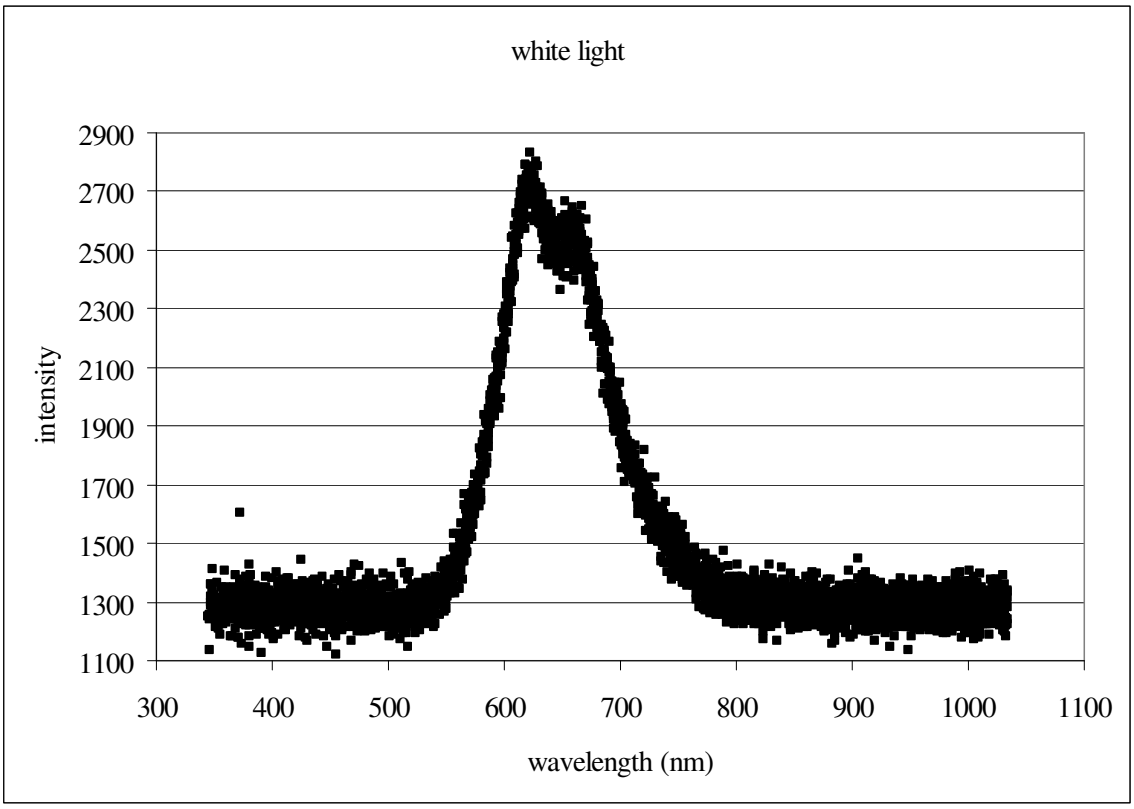

Figure 3.10. PL spectrum of the PS samples exposed to the white light source.

Environmental scanning electron microscopy images, are obtained with secondary electron detector as described in section 3.3.1, represents topographical surface structure of the samples. Images of hydrogen, blue, purple and red laser illuminated PS samples are shown in Figures 3.11 and 3.12 respectively.

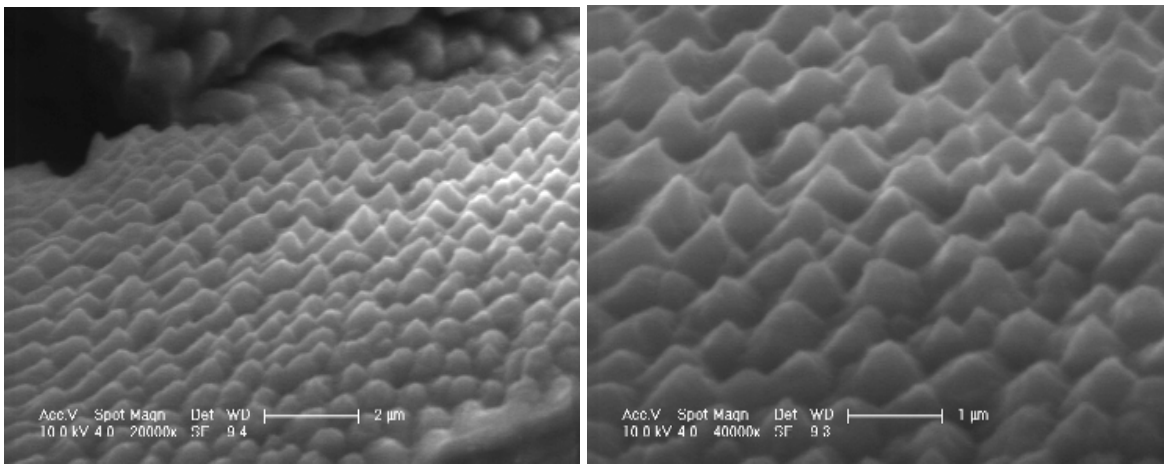

(a) ESEM images of PS samples illuminated with hydrogen laser

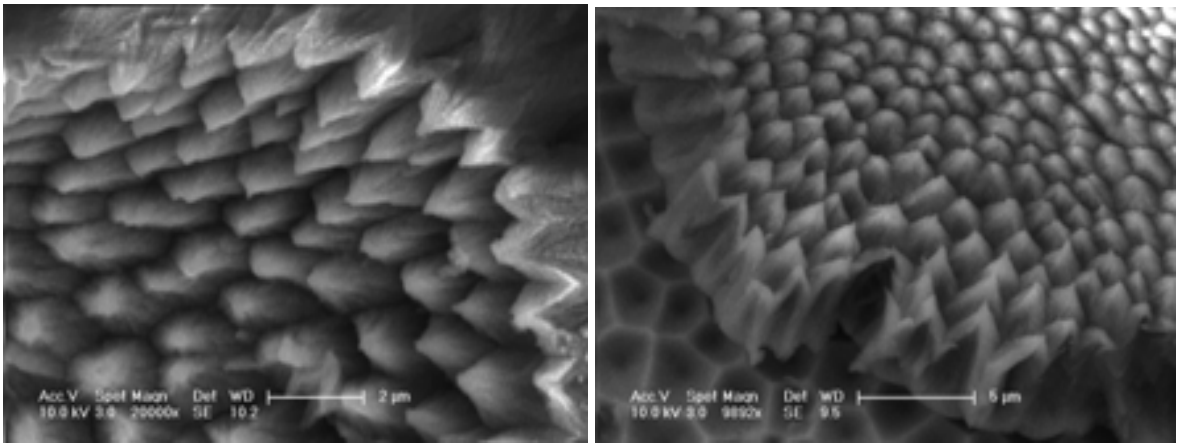

(b) ESEM images of PS samples illuminated with blue lasing diode laser

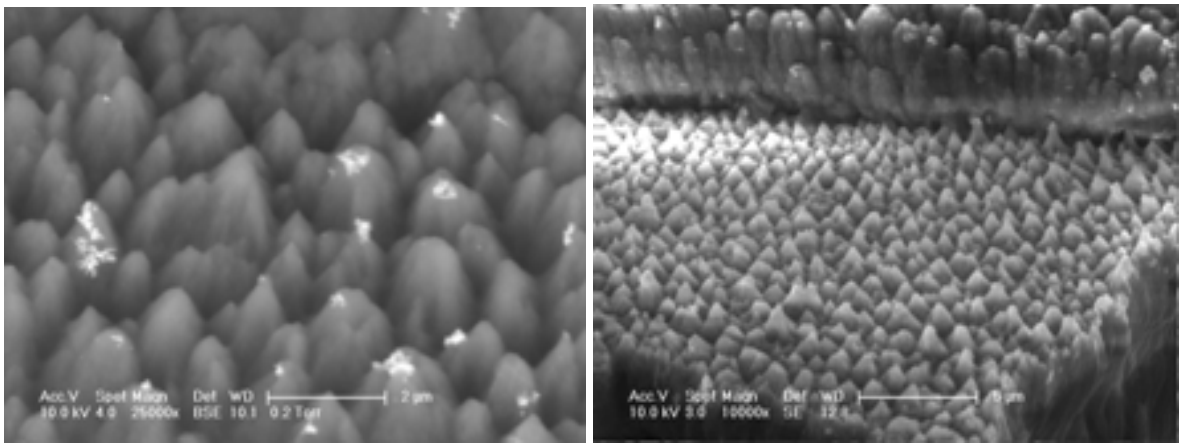

(c) ESEM images of PS samples illuminated with purple lasing diode laser

Figure 3.11. ESEM images of PS samples illuminated with hydrogen laser(a), blue lasing diode laser(b), purple lasing diode laser(c).

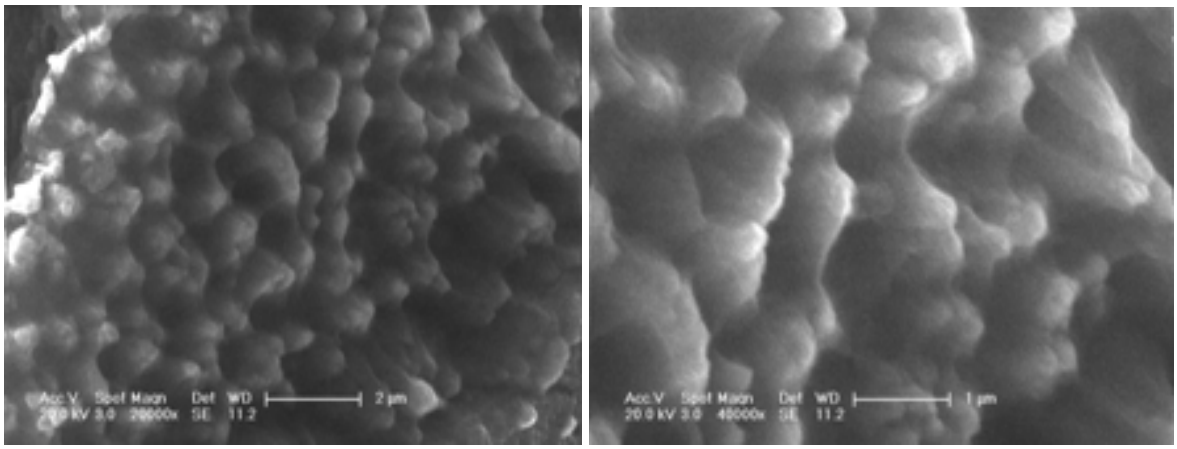

Figure 3.12. ESEM images of PS samples illuminated with red He-Ne laser.

When images are compared, the effect of the laser wavelength on porous formation can be seen directly. Laser illuminated PS is formed like regular and sharp pillar according to the studies of Kolasinsky et al. [22]. In this study, all laser illuminated PS samples are formed as pillars but there are differences between the samples in terms of size and homogeneity. Hydrogen, purple and blue laser assisted PS samples have more homogen and regular pillars than the red laser assitted one. Furthermore, in the hydrogen and purple laser assisted samples, there is a decrease in the size of the pillars when compared to those formed with the blue laser.

Figure 3.13 shows the images taken from the blue laser and blue led illuminated silicon samples to observe the effects of the coherence length on PS formation. At the blue led exposed PS, there are pores but not pillars like, on the other hand, the sample exposed to blue laser has regular and sharp pillars. Blue led enlightened PS sample is formed like white light illuminated PS as shown in Figure 3.14. When white light shows almost no coherence length, coherence length of the blue led is 0.002 mm, that is the reason for the similar PS formation.

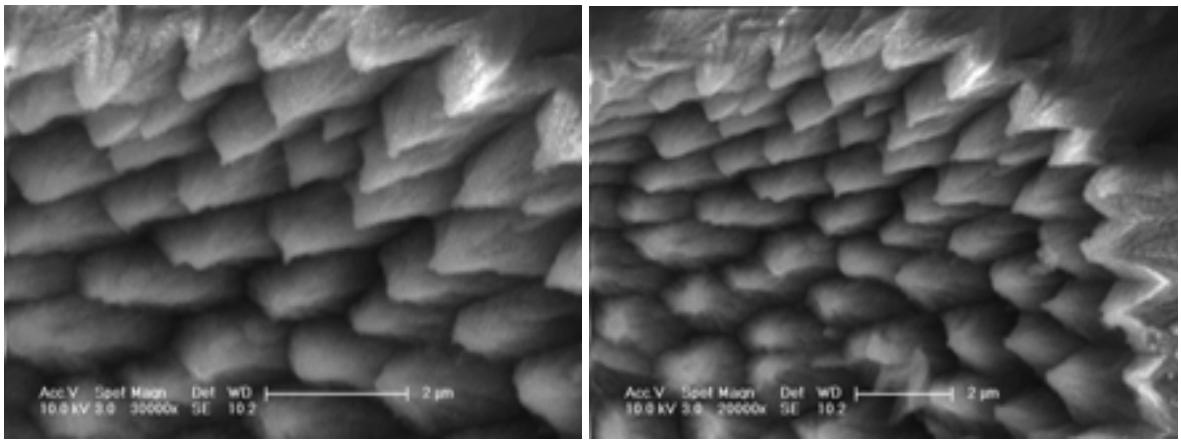

(a)

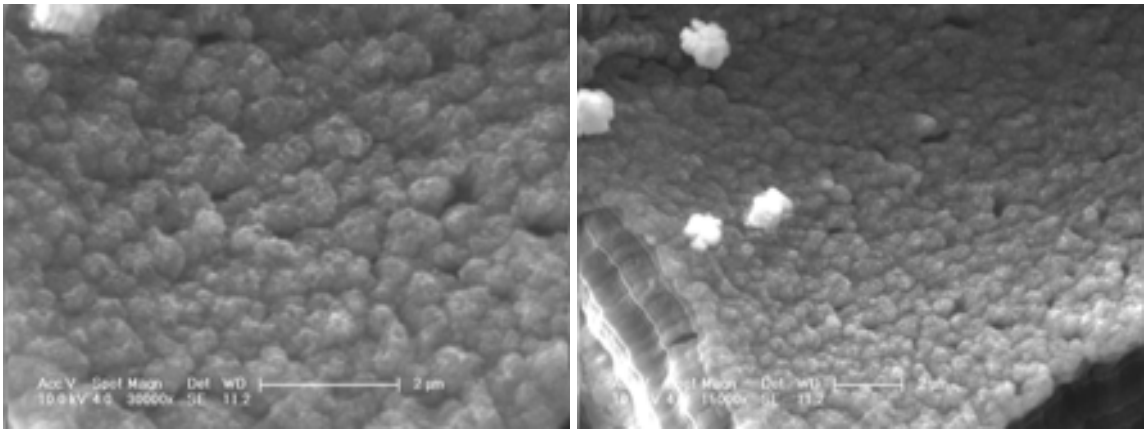

(b)

Figure 3.13. ESEM images of blue laser exposed PS sample(a) and blue led exposed PS sample(b)

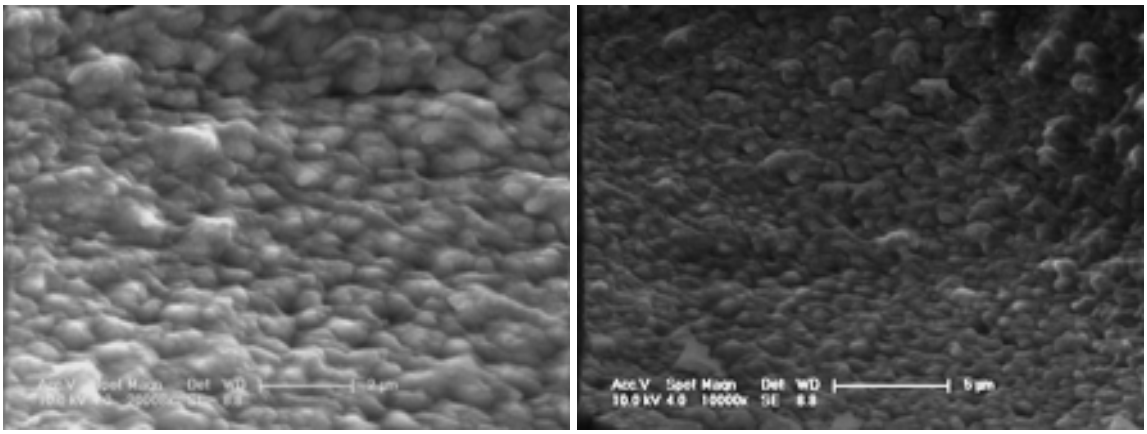

Figure 3.14. ESEM images of white light illuminated PS sample.

AFM images are taken only for the white light and blue led illuminated PS samples, since the laser sources caused big damages at the surface of the samples. At the surface of these PS samples, cavities are formed and pillars are seen only by ESEM at the edge of the cavities. AFM tip could not scan those pillars. Surface of the other PS samples are observed to be platy and convenient to be scanned with the AFM. Porous structures of the white light and blue led exposed samples can be seen from AFM images in Figure 3.15 and 3.16. The AFM images of white light and blue led assisted PS samples support the ESEM images, that is nanostructured pores can be seen from both AFM and ESEM results.

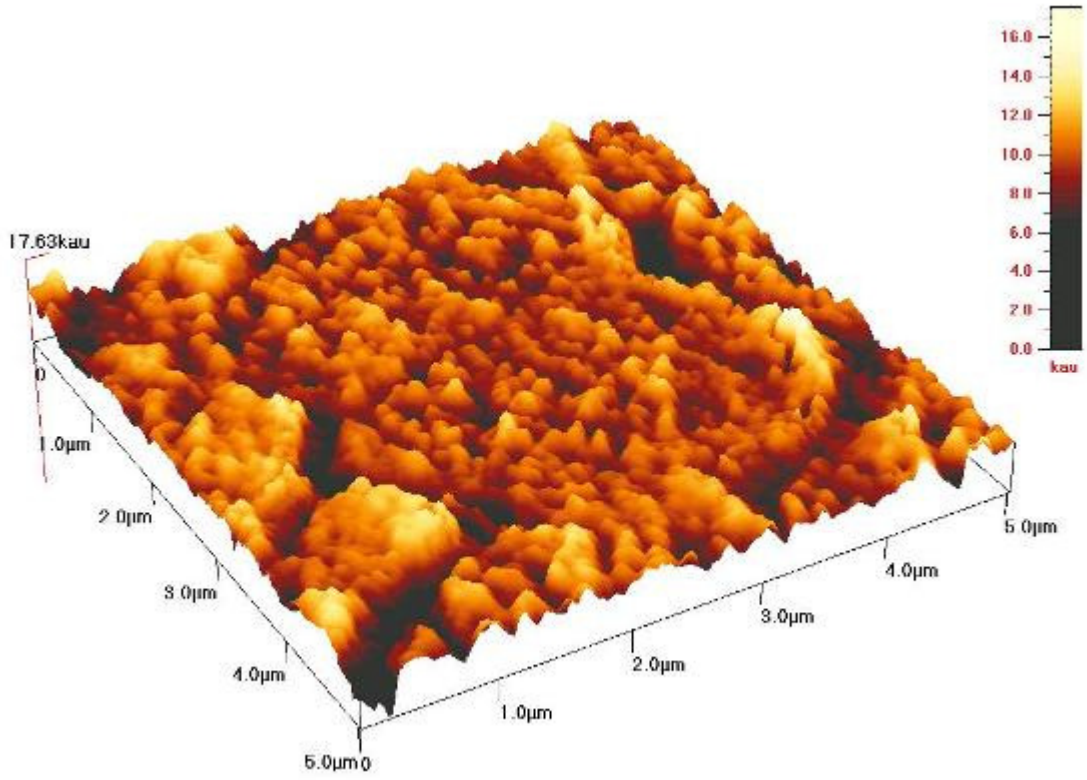

Figure 3.15. AFM images of PS samples illuminated with white light.

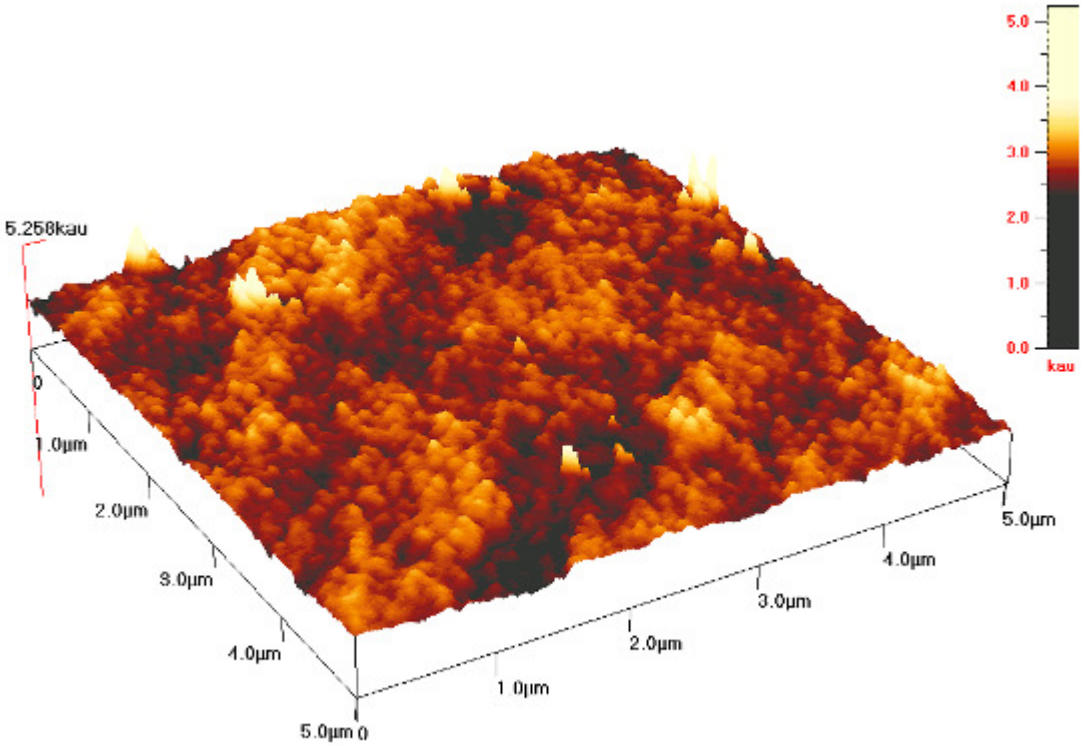

Figure 3.16. AFM images of PS samples illuminated with blue led.

4. CONCLUSIONS

In this thesis, porous silicon samples are formed under the illumination of various light sources; such as blue and purple lasing diode lasers, red lasing He-Ne laser, hydrogen laser, blue led and white light source. Optical properties of these samples are investigated by PL spectroscopy and structural properties are investigated by ESEM and AFM.

There are many parameters which affect the formation of PS. Although, most of the parameters are kept constant during anodization of the samples, cracks and different layers are formed at the PS surface as seen in the images due to the drying technique.

The PL spectra of all samples have luminescence peak almost at the same wavelength around 650-700 nm. Thus, it is obvious that in the structure of the samples, nanopores are formed, which is a requirement for the quantum confinement effect. The PL peak intensity of the white light and blue led illuminated PS samples are higher than the laser illuminated PS samples. The reason of the intensity difference is the structure dependent and this can be directly seen from the ESEM images in Figure 3.7. White light and blue led exposed samples have dense porous structure in the nanometer scale, but silicon samples formed with lasers have relatively less dense pillar structure. In the pillar structure, luminescence occurs at the sharp tips of the pillars since these tips are in the nanometer scale. In fact, the quantum confinement effect is achieved through these tips.

Additionally, according to the ESEM images, pillar formations in the laser assisted silicon nano-structures have a decrease in the size of the pillars and more regular pillars are formed with decreasing laser wavelengths. Blue laser which has 467 nm wavelength and the blue laser assisted PS have regular pillars than the red laser asisted PS. Also, hydrogen and purple laser illuminated PS samples are formed as pillars and they are much smaller then the blue laser assisted PS. In Table 4.1 homogeneity and size changes of the pillars are given in accordance with laser wavelengths.

Table 4.1. Homogeneity and size distrubution of pillars according to the laser wavelengths

	Hydrogen laser	Purple laser	Blue laser	Red laser
Wavelength	337 nm	405 nm	467 nm	633 nm
Pillar size (approx.)	352.21 nm	517.82 nm	642.63 nm	677.91 nm
Homogeneity	Homogeneous	Homogeneous	Homogeneous	Inhomogeneous

Approximate pillar size, an average value, is calculated from the ESEM images. Eventually, PS samples illuminated with short wavelength laser light have dense conical pillars with sharp tips. The pillar size decreases with decreasing laser wavelength and the tips of the pillars are sharpened in the lower wavelength illuminated PS samples. The effect of the coherence lenght also can be explained from the ESEM images. Both blue led and blue laser illuminated samples have pores in nanometer scale according to the PL results. But, blue laser illumination of the sample with long coherence lenght value is formed as conical pillars instead of the pores. The long coherence length affects the surface more intensely than the short coherence length.

For a future work, radiative life time measurements can be studied and also, x-ray diffraction measurements should be performed to investigate the crystallographic changes after PS formation.

REFERENCES

1. Canham, L. T. , “Silicon Quantum Wire Array Fabrication by Electrochemical and Chemical Dissolution of Wafers”, *Appl. Phys. Lett.*, Vol. 57, pp.1046, 1990.

2. Fauchet, P. M and J.Behren, “The strong visible luminescence in porous silicon: quantum confinement, not oxide-related defects”, *Physica Status Solidi*, Vol 204, No. 1, pp. 3-583, 1997.

3. Chi, N., Phillips, D. L. and K.Y. Chan., “In situ photoluminescence characterization of porous silicon formation”, *Thin Solid Films*, Vol. 342, No:1-2, pp. 142-147, 1999

4. Kolasinski, K.W., Walner, A.,Neuendorf, R.,Pedersen, C.X and R.E. Palmer., *Central Photoluminescence from silicon nanostructures*, Lasers for Science Facility Annual Report, Science & Technology Facilities Council, UK, 2000/2001.

5. Kolasinski, K. W., Mills D. and M. Nahidi, “Laser assisted and wet chemical etching of silicon nanostructures”, *Journal of vacuum science and technology*, Vol. 24, No. 4, pp. 1474-1479, July 2006.

6. Kolasinski, K. W and D. Mills, “Non-lithographic method of forming ordered arrays of silicon pillars and macropores”, *Journal of Physics D. Applied Physics,* Vol.38, pp.632-636, February 2005.

7. Ossicini, S., Pavesi, L. and F. Priolo, *Light Emitting Silicon for Microphotonics*, Springer, 2003.

8. Canham, L., *Properties of Porous Silicon*, Institution of Engineering and Technology, 1997.

9. Pavesi, L., Mazzoleni, C., Guardini, R., Cazzanelli, M., Pellegrini, V. and A. Tredicucci, "*Porous Silicon Microcavities",* II Nuovo Cimento, Vol.18D, pp. 1213, 1996.

10. Cullis, A.G., Canham, L.T. and P. D. J. Calcott, "The structural and luminescence properties of porous silicon", *Journal of Applied Physics,* Vol.83, Issue 3, pp. 909-961, August 1997.

11. ***Gerischer, H.,*** "The impact of semiconductors on the concepts of ***electrochemistry",*** **Electrochim. Acta, *Vol. 35*,** No. 11/12, pp. 1677 – 1699, 1990.

12. Pankove, J.I., *Optical Processes in Semiconductors*, Dover Publications, 1975.

13. Pavesi, L. and D. J. Lockwood, *Silicon Photonics*, Springer, 2004.

14. Bettotti, P., Cazzanelli, M., Dal Negro, L., Danese, B., Gaburro, Z., Oton, C. J., Vijaya P. G. and L. Pavesi, "Silicon nanostructures for photonics", *Journal of Physics:Condensed Matter*, Vol. 1, pp. 103-112, 2002.

15. Ossicini, S., Pavesi,L., Priolo,F. and S. Ossicini, *Light Emitting Silicon for Microphotonics*, Springer, 2004.

16. Hecht, E., *Optics*, Addison Wesley, 2001.

17. Kasap, S. O., *Optoelectronics and Photonics,* Prentice-Hall, 2001.

18. Canham, L., *Properties of Porous Silicon*, Institution of Engineering and Technology, 1997.

19. Bilen, B., Açıkgöz, S., Aktaş, G. and M.N. İnci, "Radiative decay rate measurement of perylene dye molecules embedded to porous silicon nano-structures", Boğaziçi University, 2009.

20. Saleh, B.E.A. and M.C. Teich, *Fundamentals of Photonics,* Wiley, 1991.

21. Yariv, A., *Optical Electronics,*Holt McDougal, 1985.

22. Mills, D. and K.W. Kolasinski, "Laser etched silicon pillars and their porosification", *Journal of Vacuum Science Tech.*,Vol. 22, Issue 4, pp. 1647-1651, 2004.